Science

Aqueous mineralogy and stratigraphy at and around the proposed Mawrth Vallis MSL Landing Site: New insights into the aqueous history of the region

Eldar Z. Noe Dobrea[1], Joseph Michalski[1] and Gregg Swayze[2]

[1]*Planetary Science Institute, 1700 East Fort Lowell, Suite 106, Tucson, AZ 85719, eldar@psi.edu; [2]United States Geological Survey, MS 964, Box 25046, Denver Federal Center, Denver, CO 80225*

Abstract

We have analyzed Compact Reconnaissance Imaging Spectrometer for Mars (CRISM) hyperspectral images from the region within and around the proposed Mawrth Vallis landing ellipse for the Mars Science Laboratory (MSL) rover in order to generate a mineralogical map of the units within the landing ellipse that can be used to guide MSL mission planning. Spectroscopic and morphological studies of the walls of a crater near the ellipse have allowed us to identify a stratigraphic section consisting of at least four primary compositional units including two Fe/Mg-smectite-bearing units at the bottom of the section, an Al-phyllosilicate-bearing unit above that, and in some instances, a Mg-phyllosilicate-bearing unit above that. HiRISE images of the Fe/Mg-smectite-bearing units typically show clear evidence for layering in the unbrecciated portions of the crater walls. The bedding planes are not always parallel and may exhibit truncations, ripple-like bedding and concave forms. The layers under the synclinal forms are not deformed, supporting the hypothesis that these synclinal forms are cross-sections of buried channels. The Al-phyllosilicate-bearing unit often shows evidence for an enhanced concentration of ferrous material at its base, as well as mineralogical evidence for limited exposure to acidic fluids. This unit typically presents fracture patterns near the top, and layering near the base. In the context of an impact crater wall, it is difficult to determine whether this pattern is caused by the impact itself or by some other depositional or diagenetic/pedogenic process. In addition to these minerals, we have identified material with a spectral signature consistent with either the sulfate bassanite or the zeolite analcime just east of the proposed landing ellipse. This material is associated with a unit that has a pitted-and-etched morphology and underlies the layered Fe/Mg-smectite-bearing units (although Fe/Mg-smectites are also prevalent throughout the rest of this unit). We interpret this pitting and etching to be the result of the dissolution of sulfates by groundwater activity. A variety of environmental conditions appear to be preserved within the landing ellipse, with Fe/Mg-smectites preserving evidence for more basic conditions exposed primarily in the eastern portion of the ellipse, and Al-phyllosilicates preserving evidence for more acidic conditions occurring dominantly toward the western portion of the ellipse. The boundary between these two mineralogical zones is sharp, well-exposed, and easily accessible.

Introduction

The Mawrth Vallis region is one of the four final candidate landing site for the Mars Science Laboratory (MSL). It is of particular interest as a site for exobiological studies of Mars because it presents a well-exposed and intact stratigraphic column of altered Noachian crust (Bishop et al. 2008; Mustard et al. 2008), and extensive arguments in support of the region as a field site for MSL have been presented by Michalski et al. (2010). Past spectroscopic studies using data from the Compact Reconnaissance Imaging Spectrometer for Mars (CRISM) and the Observatoire pour la Mineralogie,

l'Eau, les Glaces, et l'Activité (OMEGA) have revealed large (10 – 100 km long) exposures of layered phyllosilicate-bearing rocks (Michalski and Noe Dobrea 2007). Stratigraphy is not only defined by lithologic contacts, but also by mineralogy, with Al-phyllosilicate-bearing units (*e.g.* Al-smectite and kaolinite-group minerals) overlying Fe/Mg-phyllosilicate bearing units (Bishop et al. 2008; Wray et al. 2008; McKeown et al. 2009; Noe Dobrea et al. 2010). While the landing ellipse was chosen because it represents an excellent exposure of eroded, altered crust, the mineralogical diversity, stratigraphy, and morphology observed around the landing site is actually observed in outcrops throughout the western Arabia Terra region at length scales of over 1000 km (Noe Dobrea et al. 2010). This suggests that the process responsible for the formation of these rock units operated on a regional scale. It is important to note, however, that the processes responsible for the deposition of the rock units themselves were not necessarily the same processes responsible for their hydration and observed mineralogy. Proposed depositional processes include emplacement of ejecta by multiple impacts, sedimentation in fluvio-lacustrine or marine settings, and airfall of dust, volcaniclastic material, or impact-generated fines (Michalski and Noe Dobrea 2007). Additional proposed processes for the formation of the observed hydrated minerals and their stratigraphy include climate-driven top-down alteration, fluvio-lacustrine deposition, and subsurface diagenesis of clastic materials (*e.g.*, Michalski and Noe Dobrea 2007; McKeown et al. 2009; Noe Dobrea et al. 2010).

Studies of the phyllosilicate bearing-units found inside the proposed landing ellipse must be made in the context of regional and local geological and mineralogical studies. Original OMEGA observations of the region revealed the presence of two primary rock units: a Fe/Mg smectite-bearing unit, and an aluminous clay unit, originally interpreted as Al-smectite (Poulet et al. 2005). Subsequent investigations using CRISM showed that the aluminous clay unit is in fact compositionally diverse and displays evidence for Al-smectites spanning the montmorillonite - beidellite series (Noe Dobrea et al. 2010), kaolinite-group minerals, and hydrated silica (Bishop et al. 2008; McKeown et al. 2009; Noe Dobrea et al. 2010). The analysis also showed that this unit is a few 10's of meters thick, and that where observed in the region, it overlays the Fe/Mg-smectite-bearing unit. Additionally, the same stratigraphic sequence is repeated in outcrop units throughout western Arabia Terra, more than 1000 km away from the mouth of Mawrth Vallis (Noe Dobrea et al. 2010).

In this paper, we show that the terrain within and around the landing ellipse displays a broader range of hydrous mineralogy than previously realized, including the presence of acid-leaching products, sulfates, and dehydrated Mg-smectites. These findings have important implications for the history of the region, and may provide important information for consideration during the MSL landing site selection process.

Datasets and Methods

We have used calibrated (calibration level TRR2) radiance factor (I/F) data from Full Resolution Targeted (FRT) CRISM observations acquired inside the ellipse (FRT000089F7, FRT0000A600, FRT0000B141, FRT0000B643, FRT0000BB59) as well as outside the ellipse (FRT000094F6) (Figure 1). An atmospheric opacity correction was performed using two different techniques: the standard volcano scan technique (Langevin et al. 2005), and a newly derived technique based on emission phase function (EPF) observation sequences, which is summarized below.

The EPF-based technique uses nested images acquired of the same area at multiple emission angles (up to about 70°) as the spacecraft approaches the target. In principle, the airmass is proportional to the cosine of the emission angle, which allows the derivation of opacity spectra via linear regression to replace the volcano-scan opacity spectra used in the first technique. In contrast to the volcano-scan correction, the EPF technique of extracting the opacity spectrum from the same region of an observation at the time of the observation does account for temporal and spatial variations in water vapor and CO_2 column abundance. This is particularly important for accurate correction of the 2-μm CO_2 band, which partially overlaps absorptions from H_2O vapor. Multiple empirical approaches have been used to produce an opacity spectrum from the EFP sequence that has adequate signal-to-noise (S/N) ratios for removal of atmospheric gas absorptions, and that also accounts for the column-dependence on the central wavelength for each channel in CRISM data. These methods included taking ratios of spectra from the same column but at different emission angles, as well as performing a linear regression of I/F to extrapolate to zero airmass. However, neither of these methods results in opacity spectra with adequate S/N ratios for variety or reasons. In contrast, we have found that simple
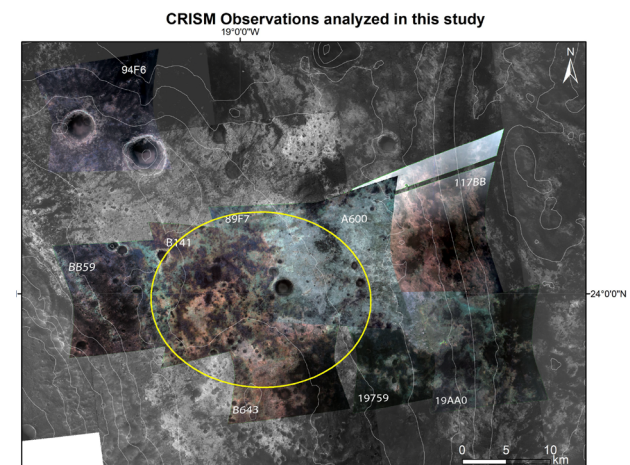

Figure 1. RGB (R=1.08, G=1.51, and B=2.51 nm) composites of the CRISM images used in this study overlaid onto a CTX base map. Strata on the walls of the two craters in FRT000094F6 are very well exposed and were used to determine the stratigraphy of the units within the landing ellipse (yellow oval). Contour intervals are set every 100 meters. (figure1.jpg)

method of averaging I/F over each column, combined with continuum correction of each spectral segment known to contain atmospheric absorptions due to CO_2, H_2O, and CO gases, and setting all non-absorption spectral regions to unity, results in opacity spectra with high enough S/N for use as in atmospheric corrections.

The removal of atmospheric absorptions from the spectra uses the same technique described in Langevin et al. (2005), where the EPF-derived opacity is used in place of the volcano-scan derived opacity. The use of a locally derived atmospheric opacity spectrum that provides a better estimate of the relative opacities of CO_2, H_2O (water and ice), and CO for each specific observation, results in a more accurate atmospheric correction compared to the volcano scan technique. Comparison between the volcano-scan and the EPF-based techniques shows that the EPF technique significantly improves the correction of the 2-µm CO_2 absorption triplet, and hence allows the identification of the 1.9-µm hydration band without the need ratio the spectra of areas of interest to the those of spectrally bland areas (Figure 2). Avoiding the use of spectral flat fielding results in spectra with higher S/N ratios. This in turn, allows the identification of weaker bands and makes direct comparison between separate observations taken at similar dust and water-ice opacities possible.

Subsequent data processing includes destriping and despiking (Parente et al. 2008), as well as parameterization (*e.g.* Pelkey et al. 2007; Ehlman et al. 2009) that is used to identify and map spectrally interesting units. In some cases, comparisons between spectra were made by taking ratios of the spectra of interest to the known spectrally neutral units in the same column of observation in order to remove artifacts that may be introduced by potential column-dependent systematic errors, and to develop confidence in our detections.

HiRISE map-projected images overlapping with the CRISM data were also used in order to characterize meter-scale morphology and surface texture. This part of the study focused on HiRISE image PSP_004052_2045.

Results

Local stratigraphy inferred from nearby craters

Compared to the rest of the Mawrth Vallis region, materials within the landing ellipse exhibit some of the strongest spectral hydration features, and are seemingly the least resistant to erosion (Michalski and Noe Dobrea 2007). The stratigraphic distribution of units within the landing ellipse can be difficult to infer due to the fact that the total change in elevation over the major axis of the landing ellipse (25 km) is only about 300 meters and topographic variations are therefore subtle. Additionally, remote sensing studies of stratigraphy using craters within the ellipse can be difficult because many of them have been topographically inverted by the same erosional processes that have exposed the
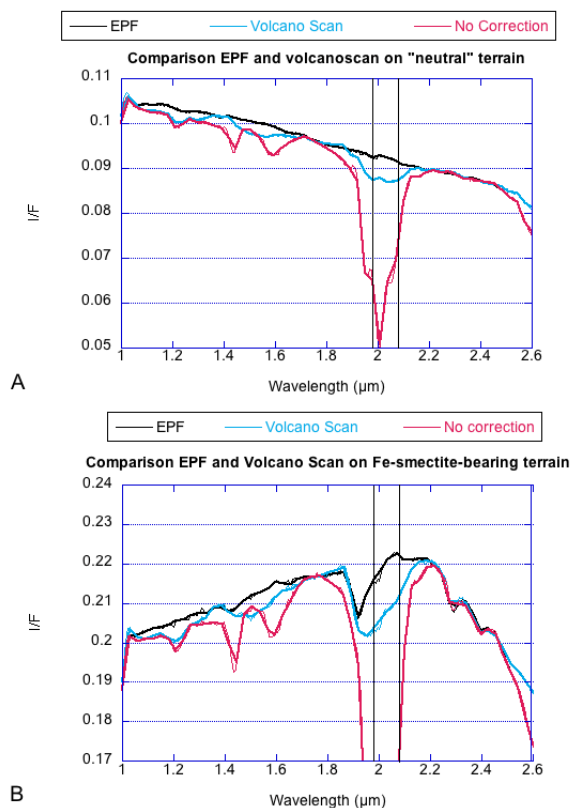

Figure 2. (a) Comparison of EPF and volcano scan atmospheric correction techniques with atmospherically uncorrected CRISM spectra of "neutral" terrain. Although not perfect in the 1.98-2.08 µm region (bounded by vertical lines), the EPF technique is an order-of-magnitude more accurate than the volcano scan technique in correcting the 2-µm CO_2 triplet. Note also the systematic noise imparted by the volcano scan technique in the 1-1.8 µm region. (b) Comparison of EPF and volcano scan atmospheric correction techniques with atmospherically uncorrected CRISM spectra of Fe-smectite-bearing terrain. Note the appearance 1.9 µm band, which is occluded by systematic errors in the volcano scan technique. In all cases, original spectra are shown as thin lines overlaid by the smoothed spectra using heavier lines. (figure2a.gif) (figure2b.gif)

phyllosilicate-bearing units. However, there are two craters located about 18 km northwest from the center of the landing ellipse that present excellent exposures of the regional stratigraphy in their walls. We therefore focus our analyses on the stratigraphy exposed in the walls of these craters and the surrounding terrain, and assume that the stratigraphy within the landing ellipse will be similar to that observed in the crater walls.

The CRISM FRT000094F6 image cube covers both craters which are about 3.9 and 3.7 km in diameter and have the provisional names of Llanfyllin (24.26 N, 19.18 W) and Llanfechain (24.32° N, 19.31° W), respectively. Excellent rock exposures are observed in their walls as well as in outcrops around the craters. Spectroscopic analysis of these outcrops reveals the presence of four spectral units (Table 1, Figures 3 and 4).
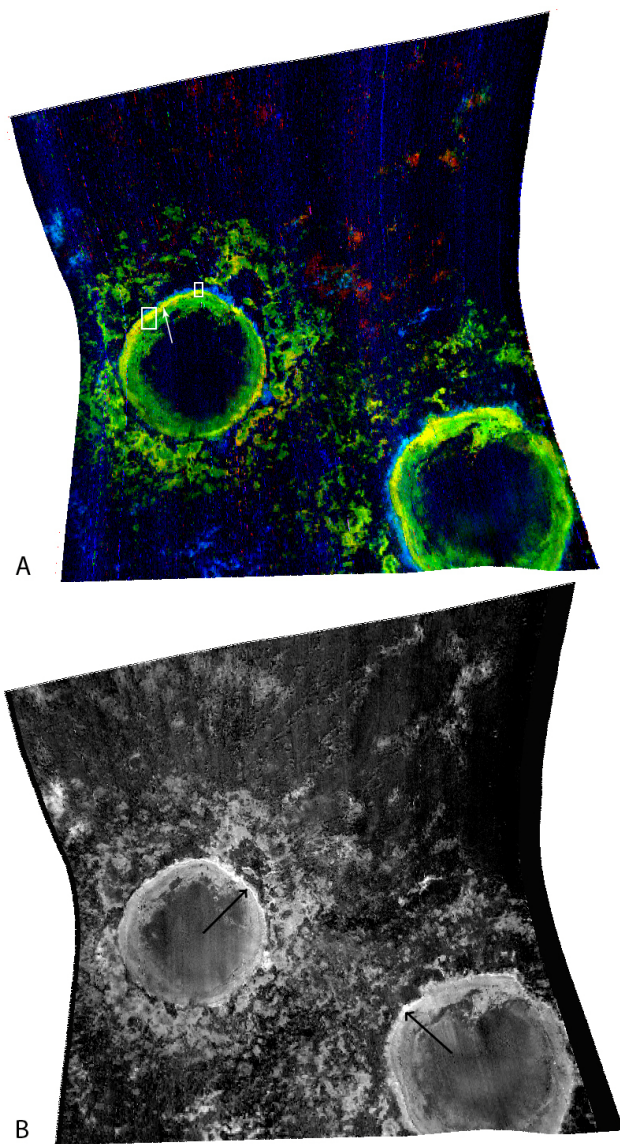
Table 1. Units identified in walls of craters and plains in the vicinity of proposed landing ellipse.

Unit # from deepest to shallowest	Bands (µm)	Mineralogical Interpretations
1	1.41-1.42 and 1.92 µm absorptions, with weak or absent bands at 2.29-2.30, 2.38-2.40 µm	Hydrate, either a mixture of Fe/Mg smectite with spectrally neutral dark component or a poorly altered rock
2	1.42, 1.92, 2.28-2.29, 2.38-2.39 µm	Fe/Mg smectites
3a	1.41-1.42, 1.92, combination of one or more bands at 2.16-2.20	Al-smectites and kaolinite-group minerals
3b	1.41-1.42, 1.90-193, combination of one or more bands at 2.16-2.21 µm plus additional absorption at 2.26-2.27 µm. 1.9 µm feature sometimes absent	Al-phyllosilicates, including kaolinite-group minerals and Al-smectites. Also either jarosite or the evaporitic residue of an acid-altered smectite.
4	2.31, weak or absent 1.9 µm feature	"Dehydrated" Mg smectite

combination bands at 2.29-2.31 and 2.38-2.40 µm in addition to an H-O-H combination band at 1.91 µm and an OH stretch overtone at 1.41-1.43 µm. The position of the Fe-OH combination band due to octahedrally coordinated Fe^{3+} in smectites is located at 2.29 µm, with the band center shifting towards longer wavelengths as the proportion of Mg:Fe^{3+} increases (*e.g.*, Bishop et al. 2008). Hence, we interpret the CRISM spectral signature as that of an Fe-smectite, probably nontronite. This contrasts with most other regions of Mars where the metal-OH combination band occurs near 2.30 µm. The primary difference between units 1 and 2 is that unit 1 has a lower albedo and often exhibits little to no absorption at 2.29-2.30 µm, suggesting that either the nontronite is less well-ordered in unit 1, or that other hydrated minerals may be intermixed with the smectite. Other hydrated minerals that could reasonably occur in the region and which do not exhibit significant absorptions other than at 1.4, 1.9, and 2.4 µm within the 1 - 2.5 µm region are some polyhdrated sulfates (*e.g.*, Mg- and Fe-sulfates) and ferrihydrite. Polyhydrated sulfates have been observed elsewhere on the planet (*e.g.*, Mangold et al. 2008; Noe Dobrea et al. 2008; Bishop et al. 2009). These sulfates typically exhibit hydration absorption features around 1.44, 1.94, and 2.40 µm. Many of the polyhydrated sulfates observed thus far on Mars have similar absorptions, and their hydration band is typically centered at wavelengths beyond 1.93 µm. Ferrihydrite also exhibits a weak absorption around 1.43 µm, a sharp absorption at 1.93 µm, and a broad absorption centered around 2.41 µm. Based on the position of the 1.9 µm band, we infer that the spectral features in unit 1 are probably not due to polyhdrated sulfates or ferrihydrite, but are likely due to poorly sorted and potentially dehydroxylated clays.

HiRISE observations of the transition from units 1 and 2 (Figure 6) often show the presence of a distinct boundary between the darker unit 1 and the lighter-toned unit 2. In
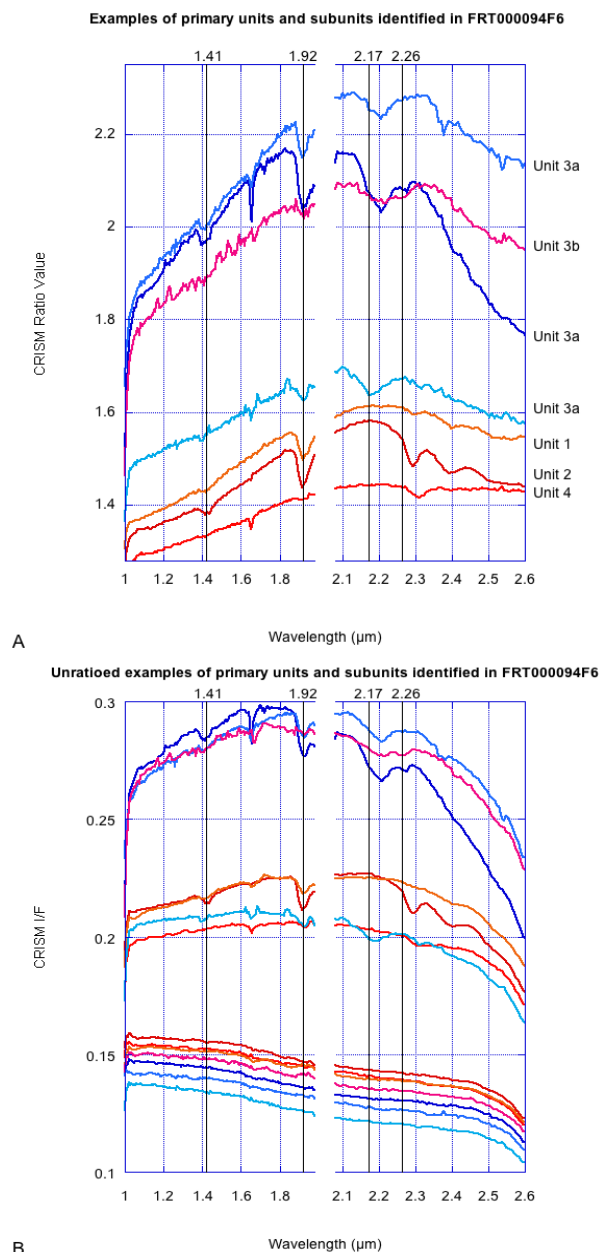
Figure 3. (A) RGB composite of parameter maps for D2300, BD1900R, and BD2200 in the CRISM analysis tools. The minimum threshold is set at 0 for all three channels. In this image, unit 1 is green, unit 2 is yellow, unit 3 is blue, and unit 4 is red. Large and small white boxes outline locations of Figures 6a and b, respectively. White arrow indicates location of Figure 7. (B) OLINDEX2 parameter map showing the distribution of material with a 1-µm region ferrous slope. The distribution of ferrous material correlates well with the distribution of hydrated material. An unusually high concentration of this material occurs in a discrete layer near the top of the stratigraphic sequence in the walls of both craters (black arrows). CRISM image FRT000094F6. North is up, image is 10 km across.

Units 1 and 2 are shown in green and yellow, respectively, in Figure 3, and correlate primarily with the craters' walls and ejecta. Unit 3 (cyan-blue) and correlates to the craters' rims and patchy areas in the plains units. Unit 4 (red) correlates with isolated patches on the plains units.

The spectra of units 1 and 2 are consistent with the spectra of Fe/Mg phyllosilicates (Figure 5), which have metal-OH

Examples of primary units and subunits identified in FRT000094F6

Unratioed examples of primary units and subunits identified in FRT000094F6

Figure 4. (A) Sample ratio spectra of 5 units identified in FRT000094F6. Note correlation between decreased spectral ratio value and spectral contrast of bands in unit 1 compared to unit 2. Spectra with red tones are 9x9 pixel averages from Units 1,2, and 4, spectra with blue tones are from subunit 3a are 3x3 pixel average, and magenta spectrum is from subnit 3b and is a 3x3 pixel average. The smaller pixel averages were necessary due to the greater spatial variability in those stratigraphic units. (B) Numerator and denominator spectra for ratioed spectra shown in A. Color-coding is the same for both plots. (figure4a.gif) (figure4b.gif)

many cases, the transition from unit 1 to unit 2 also corresponds to a transition from highly brecciated material to less fractured material. Both units appear layered in many places at HiRISE scales. Although the beds are often parallel, there are several examples of layer truncations and concave-
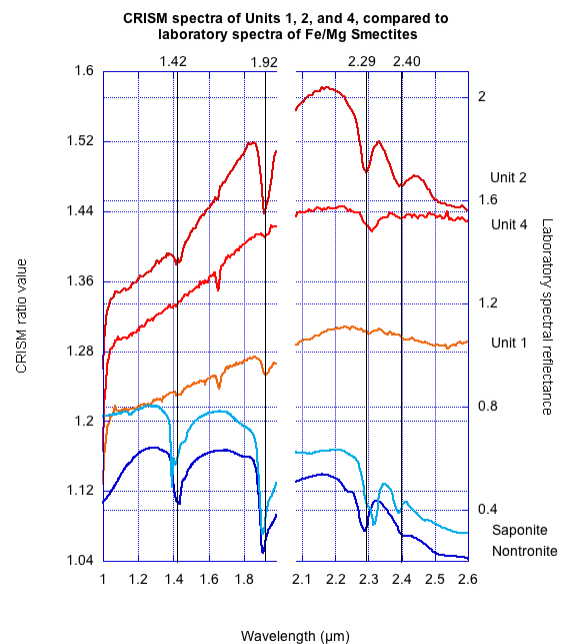
CRISM spectra of Units 1, 2, and 4, compared to laboratory spectra of Fe/Mg Smectites

Figure 5. Comparison of CRISM spectra from units 1, 2, and 4 (tones of red) to laboratory spectra of Fe-smectites (nontronite) and Mg-smectites (saponite). Spectra from nontronite CBJB26 and saponite LASA51 are from the CRISM Spectral Library. (figure5.gif)

up bedding structures in unit 2 that suggest the presence of a dynamic environment during their deposition (*e.g.*, Wray et al. 2010) (Figure 7).

The spectra of subunit 3a are consistent with the presence of a combination of Al-smectites and kaolinite-group minerals (Figure 8). Al-smectites have a single absorption in the 2.19-2.21-µm region in addition to an H-O-H combination band at 1.91 µm and an OH stretch overtone at 1.41 µm. The kaolinite-group minerals have a doublet absorption at 2.16-1.17 and 2.19-2.20 µm as well as a doublet at 1.39 and 1.41 µm. Kaolinite-group minerals generally do not have residual tetrahedral layer charge, and therefore do not contain interlayer water or interlayer cations. The exception is halloysite, which contains some interlayer water and therefore has a hydration band near 1.9 µm (*e.g.*, Churchman and Carr 1975). CRISM spectra of this unit typically have a distinctive absorption at 2.20 µm, with a weak shoulder near 2.16 µm, and a sharp absorption at 1.91 µm, suggesting that the smectites are spatially mixed with the kaolinite-group minerals. HiRISE observations of this unit show evidence for layering, particularly in the lowest layers of the unit. In contrast, the upper portion of the unit often has meter-scale polygonal fracturing. This polygonal pattern is consistent with that observed in the other Al-phyllosilicate bearing units identified throughout Mawrth Vallis and Western Arabia Terra (*e.g.*, McKeown et al. 2009; Noe Dobrea et al. 2010).

In addition to the smectite/kaolinite mixture inferred from absorptions in the 2.16-2.20 µm region, some spectra from unit 3 have an additional absorption centered near 2.26-2.27
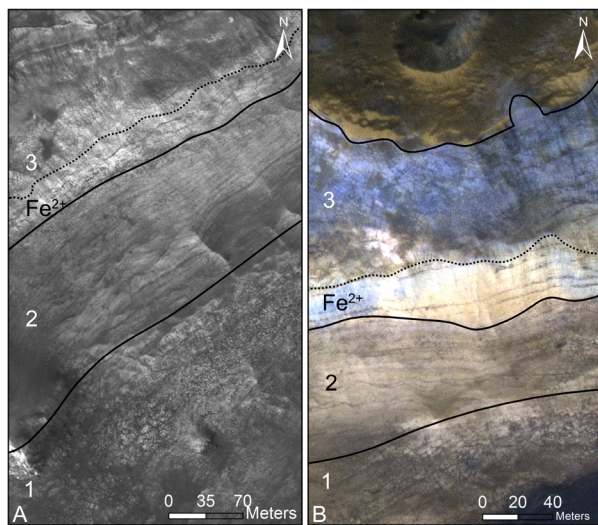
36

Figure 6. HiRISE (PSP_004052_2045) view of the 3 stratigraphic units exposed in the walls of Llanfyllin Crater. (A) HiRISE RED filter, (B) HiRISE RGB composite. Location of images is shown in Figure 3a. (figure6.jpg)
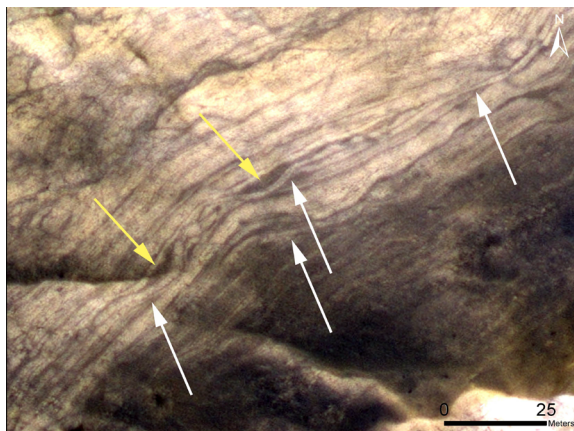

Figure 7. Examples of layer truncations (white arrows) and concave-up structures (yellow) arrows exposed in the wall of Llanfyllin Crater. Location of image is shown in Figure 3a. (figure7.jpg)

µm. Spectra with this 2.20-2.27 µm "doublet" belong to surface materials in subunit herein referred to as "unit 3b", although for the most part it is spatially mixed with unit 3 (*i.e.*, it outcrops intermittently within unit 3). Similar spectra have been identified in other parts of Mars as well, particularly in Valles Marineris, and interpreted to be a poorly crystalline Fe–SiO$_2$ phase formed either from (1) the acid leaching of a smectite or (2) neoformation from dissolved basaltic material (Roach et al. 2010; Weitz et al. 2009) (Figure 9). This interpretation is supported by leaching studies performed by Tosca et al. (2008) that show the development of a 2.27 µm absorption feature accompanied by a weaker 2.20 µm shoulder and a shift of the 1.9 µm band toward 1.93 µm when smectite samples are exposed to slightly acidic to neutral aqueous conditions for a few days to a couple of weeks.

Some single-pixel endmember spectra (defined by the depth

of the 2.26 µm feature) extracted from subunit 3b on the rim of the crater in FRT000094F6 do display a prominent band at 2.26 µm, and shoulders at 2.21, 2.46, and 2.52 µm, which are consistent with those exhibited by the spectrum of jarosite (Figure 10). Other examples of jarosite have been identified further north in the Mawrth Vallis region by Farrand et al. (2009). In addition to the 2.26 µm absorption, the CRISM ratioed spectra exhibit similarities to the jarosite spectra of Farrand et al. (2009), including an absorption feature at 1.92 µm, a slight inflection near 2.46 µm, and an absorption feature at 2.51 µm (Figure 11). However, differences exist between the spectra from these areas. In particular, the 2.26-2.27 µm and 2.46 µm features in the spectra of subunit 3b are weaker than those observed in the jarosite spectra of Farrand et al. (2009), whereas the 1.92 and 2.20 µm features are stronger in the spectra from subunit 3b. This difference suggests that this combination of spectral features is associated with an acid-alteration phase or phases, where spectral variations in relative band depths may indicate different degrees of acid-alteration throughout the scene.

Finally, the spectrum of unit 4 is unique in the region because it has a 2.31 µm absorption which is consistent with a Mg-OH combination band in phyllosilicates. However, the CRISM spectra show a weak to absent absorption at 1.9 µm, suggesting that these phyllosilicates are poorly hydrated. Spectra of this material are similar to Fe/Mg smectites, but lack their relatively strong 1.9 µm feature. The spectra are not similar to available spectra for talc, chlorite, serpentine, or other common Fe/Mg clays. However, the location of what is likely a metal-OH band at 2.31 um suggests a magnesian composition clay mineral, which could potentially correspond to poorly crystalline talc or other Mg-rich clays with limited interlayer water.

Ferrous slope. A positive spectral slope is observed in the 1-2 µm region of many of the hydrated units, the intensity of which is parameterized via the OLINDEX parameter of Pelkey et al. (2007) (Figure 3b). Materials cropping out in a thin layer at the transition between units 2 and 3 have an abnormally high (50 s greater than the mean of all units with OLINDEX > 0) OLINDEX parameter values (Figure 3b). This observation is consistent with previous studies (Bishop et al. 2008; McKeown et al. 2009; Noe Dobrea et al. 2010), where the spectral slope was interpreted as evidence for the presence of a ferrous mineral phase. The OLINDEX parameter may incorrectly map hydrated regions as Fe^{2+}-rich because of the associated decrease in reflectance beyond 2 µm. For instance, Noe Dobrea et al. (2010) proposed that variations in the strength of this spectral slope might be correlated with variations in the depth of the vibrational bands in the spectra of the hydrated units, which suggests that the observed variations in OLINDEX values are caused by mixing of the hydrated material with a darker material. Although there is some correlation between the ferrous slope and the depth of the 1.9 µm band (75% correlation) in the present study area, no such correlation is observed between the ferrous slope, the depth of the 2.2 µm band, the depth of the 2.3 µm band, or the 1 µm reflectance. This suggests that
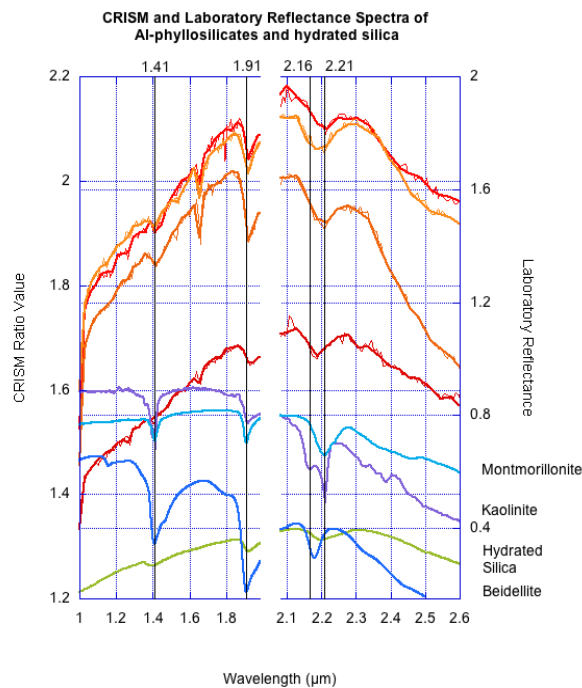
Figure 8. Comparison of CRISM spectra (tones of red) of unit 3a in FRT000094F6 to laboratory spectra of Al-smectites montmorillonite 397F013 (CRISM spectral library) and beidellite GDSGDS123 (USGS spectral library– Clark et al. 2007), kaolinite LAKA01 (CRISM spectral library), and hydrated silica (Bishop et al. 2005). (figure8.gif)

the ferrous slope is associated with a mineral other than the reported Fe/Mg-smectites or Al-phyllosilicates.

Hydrated units outside the landing ellipse. Hydrated materials are observed in every CRISM image within and adjacent to the proposed landing ellipse. In addition to the Fe/Mg- and Al-bearing phyllosilicates reported in other studies, we have also identified spectra from a region immediately east of the ellipse that exhibits hydration features at 1.4 and 1.9 µm, as well as an additional rounded absorption near 2.5 µm (Figure 12). This set of absorptions is most consistent with the sulfate bassanite or the zeolite analcime, both of which have a rounded absorption at 2.5 µm in addition to 1.4 and 1.9 µm absorptions. The spectra originate from a portion of an aerially extensive Fe/Mg phyllosilicate-bearing unit that has a pitted-and-etched morphology, which appears to underlie layered Fe/Mg-phyllosilicate bearing material (Figures 13 and 14).

Distribution of units within the landing site ellipse

Figure 15 shows spectra of units 1, 2, and 3 keyed to locations inside the landing ellipse shown in Figure 16. Unit 2 mineralogy is most abundant in the eastern side of the ellipse whereas unit 3 mineralogy is most abundant in the west side of the ellipse. There is a sharp mineralogical and morphological boundary between units 2 and 3 roughly at the center of the landing ellipse. Occurrences of unit 4 are not observed inside the landing ellipse, nor are occurrences
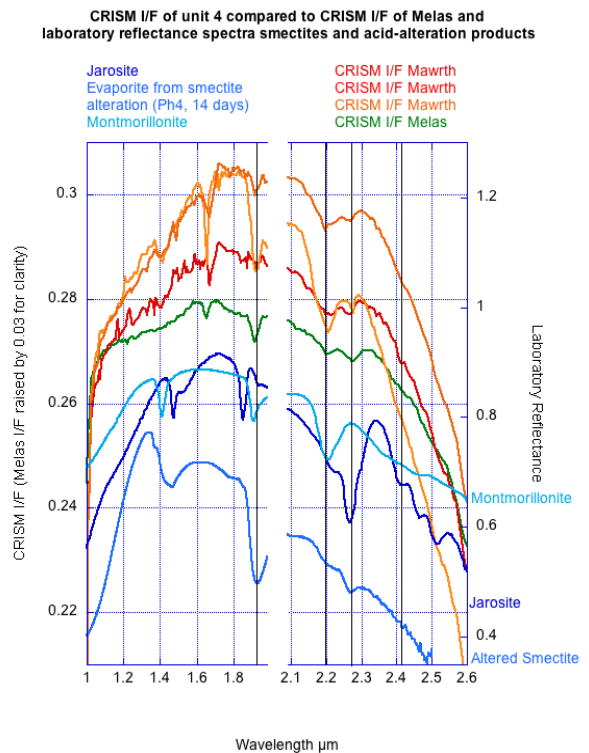

Figure 9. Comparison of unit 3b I/F CRISM spectra (tones of red) to Melas Chasma I/F spectra (green) and library spectra (tones of blue) of montmorillonite 1292F35 (CRISM spectral library), jarosite LASF30A (CRISM spectral library), and precipitate from the alteration of smectite at pH 4 for 14 days (Tosca et al. 2008). (figure9.gif)

of the 2.5 µm absorber (although instances of the pitted-and-etched morphology in which it occurs are observed in the eastern portion of the ellipse). Not all of the Fe/Mg-phyllosilicate bearing units within the ellipse present "clean" smectite spectra (characterized by diagnostic bands at 1.43, 1.91, and 2.29, and 2.39-2.41 µm). Many spectra from the same units show a decrease in the strength of the 2.29 and 2.39-2.41 µm features with no change in the 1.9 µm absorption. This is consistent with the spectral signature of unit 1.

Discussion

Our mineralogical and stratigraphic interpretations for the area northwest of the proposed landing site are consistent with previously published results (*e.g.*, Wray et al. 2010; McKeown et al. 2009). The detection of Fe/Mg smectites, Al-smecties, and kaolinite-group minerals indicate that the proposed MSL landing ellipse retains a record of temporal variations in the geochemical conditions experienced by the Mawrth Vallis region. Fe/Mg smectites are very susceptible to alteration by acidic water (*e.g.*, Altheide et al. 2010). Their presence in the eastern half of the ellipse suggests that pH conditions there were alkaline to neutral during the period of their formation, and that they were subsequently protected from exposure to putative subsequent acidic
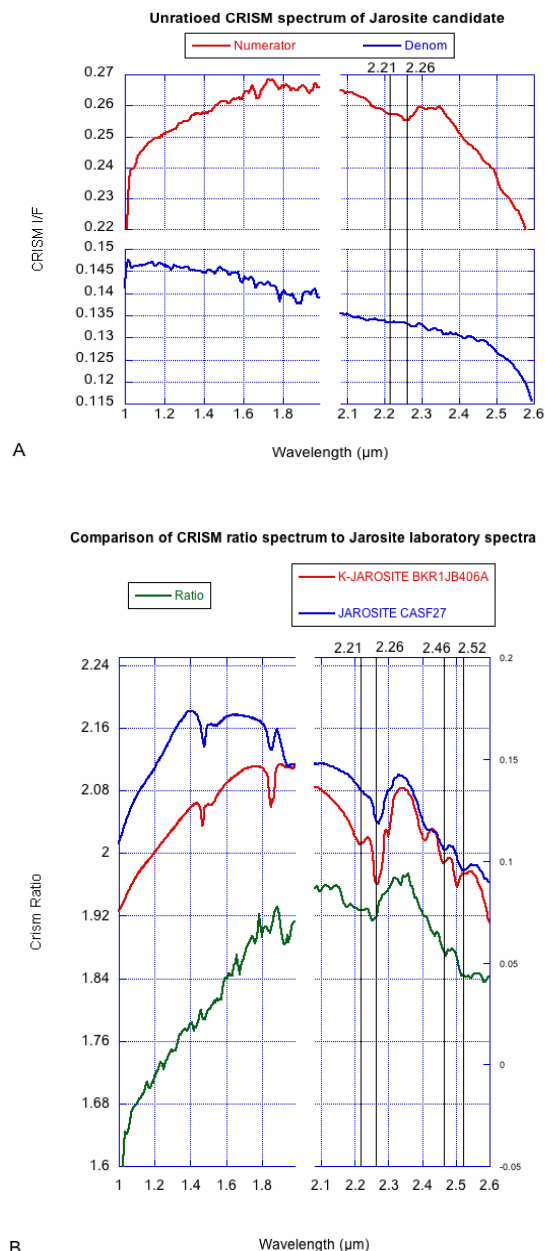
Unratioed CRISM spectrum of Jarosite candidate

A

Wavelength (µm)

Comparison of CRISM ratio spectrum to Jarosite laboratory spectra

B

Wavelength (µm)

Figure 10. Single-pixel (18x18 m) CRISM endmember spectrum extracted from subunit 3b on the rim of the crater in FRT000094F6. (A) Numerator and denominator spectra from a 2.26 µm endmember pixel and spectrally bland pixel, respectively. (B) Ratioed spectrum compared to jarosites from the CRISM spectral library. CRISM spectrum displays absorptions at 2.26, 2.46, and 2.52 µm characteristic of jarosite. (figure10a.gif) (figure10b.gif)

conditions. Absorptions observed at 2.20 and 2.27 µm in the spectra of the Al-phyllosilicate bearing unit are consistent with absorptions observed in the evaporitic residue of solutions formed from low-grade leaching of phyllosilicates by mild acidic solutions (*e.g.*, Tosca et al. 2008; Roach et al. 2010). Hence, the presence of these alteration products

suggests that at least part of the Al-phyllosilicate bearing unit might be a product of exposure to acidic conditions at some point after its formation, while the underlying Fe/Mg-phyllosilicate-bearing unit was protected from these acidic conditions. This is further supported by the putative presence of kaolinite mixed with the Al-smectites either in a physical mixture, or as part of a mixed-layer unit. A reasonable interpretation is that the Al-phyllosilicate bearing unit was probably once Fe/Mg smectite rich but was subjected to acid leaching, which formed a residual crust rich in Al-phyllosilicates that preserved underlying pH-sensitive Fe/Mg smectites from further alteration. Acidic conditions were ephemeral as current exposures of Fe/Mg smectite rich rocks would not exist if conditions remained acidic. The Al-phyllosilicate rich acid-leached crust was subsequently eroded in places, exposing underlying Fe/Mg smectite units.

The detection of a 2.20-2.27 µm doublet is also intriguing because it could potentially help explain spectral results from the MGS Thermal Emission Spectrometer (TES). TES spectra of the phyllosilicate-bearing surfaces at Mawrth Vallis are dominated by aluminous or ferric silica (Michalski and Fergason 2009). If weathering of the clays has resulted in silica-rich coatings, this could result in a dominant thermal IR spectral component, even if the coatings are thin ($< 5\,\mu m$) (Kraft et al. 2003). Therefore, acid weathering may have resulted in free silica coatings that are detectable by TES.

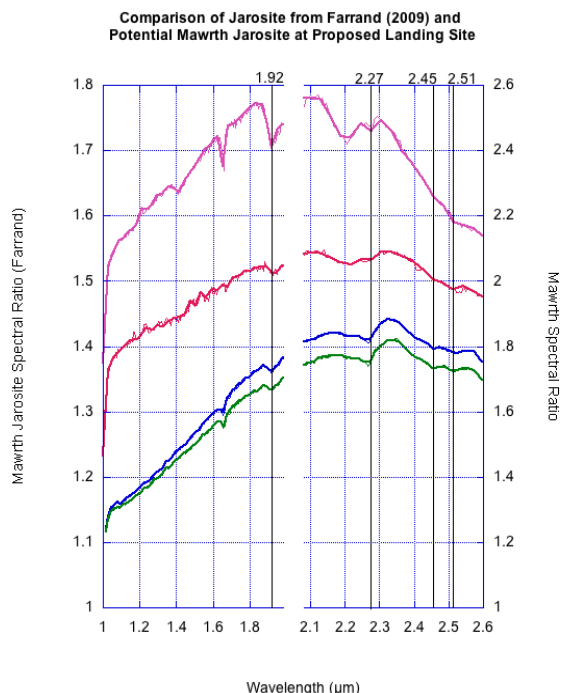These observations suggest that the proposed Mawrth Vallis

Comparison of Jarosite from Farrand (2009) and Potential Mawrth Jarosite at Proposed Landing Site

Wavelength (µm)

Figure 11. Comparison of CRISM spectra of the 2.20, 2.27 µm absorber identified at and near the proposed MSL landing ellipse (tones of red) to the CRISM spectra of jarosite identified by Farrand et al. (2009) (blue and green). (figure11.gif)

landing site may preserve a stratigraphic record of initially neutral conditions, represented by lower Fe/Mg smectite rich units erosionally exposed on the eastern side of landing ellipse, followed by acid-leaching conditions, represented by an upper Al-phyllosilicate rich unit preserved as a paleosurface on the western side of the ellipse. Hence, the

Figure 12. (A) Comparison of CRISM ratio spectra to laboratory reflectance spectra of the sulfate bassanite GDS145 (Clark et al. 2007) and the zeolite analcime GDS1 (Clark et al. 2007). (B) Comparison of continuum-removed CRISM ratioed spectra to the continuum removed reflectance spectra of the same bassanite and analcime as in (A). (figure12a.gif) (figure12b.gif)

landing site may capture all of the major epochs of Martian alteration proposed by Bibring et al. (2006). An east-west traverse of the ellipse would therefore allow us to study important portions of ancient Martian history, including rocks from the phyllosilicate-forming era that may preserve evidence of past organics, but also rocks from a subsequent acidic. The boundary between these two eras exists within the ellipse and *in situ* studies of the mineral assemblages, bedding, and textures there may allow us to undersand the environmental conditions that led to the acidification of the martian surface at the end of the Noachian.

The specific mineralogy of the material displaying an absorption feature at 2.5 µm cannot be uniquely constrained at this time using spectral studies alone. However, bassanite has been identified by Wray et al. (2010) further north within Mawrth Vallis, and some additional constraints are suggested based on the morphology of the unit that the 2.5 µm absorber is associated with. The pitted-and-etched terrain in which this material is found exhibits closed pits partially lined with residual boulders. The absence of rims and dunes, the presence of boulder-strewn interiors, and sharp edges suggest that these pits were not produced by impacts or aeolian deflation, and are therefore interpreted here to result from collapse associated to subsurface volume loss, presumably by dissolution (Figure 14). Sulfates have a much higher solubility than zeolites, and their dissolution could create subtantial subsurface volume loss. Hence, the pitted-and-etched morphology suggests the presence of sulfates, immediately east of the ellipse.

An alternative for the volume loss is the dehydration of gypsum to bassanite under burial conditions. The triple point for the gypsum-bassanite-anhydrite system occurs at about 80.5°C and 235 MPa, which on Mars would require burial depths of about 20 km (Mirwald et al. 2008) in the absence of an unusual thermal gradient. However, bassanite has also been produced by the dehydration of gypsum in the laboratory at temperature of 24°C and ~0.8 Pa P_{H_2O} (Chipera and Vaniman 2007). Hence, although we find it likely that sulfates are responsible for the volume loss, it is not possible to constrain at this time whether the pits were formed by the dissolution of bassanite or the dehydration of gypsum.

The tentative identification of bassanite in the pitted-and-etched unit is of particular interest because this sulfates would need to be a substantial part of the original unit rather than a pore-filling phase in in order for the pits to form from structural failure during dissolution. Accordingly, this suggests the deposition of a sedimentary sulfate-bearing unit before or during the deposition of the clay-bearing units.

Within the ellipse, the eastern portion is of great interest because it contains the largest areal exposure of the unaltered Fe/Mg smectites, and hence preserves evidence of the "neutral" period of clay formation and deposition. Many of the spectra from this area are excellent matches to the spectra of laboratory Fe/Mg smectite samples, suggesting that they have not been exposed to alteration by acidic fluids or burial metamorphism, both of which would alter them. Organics are also sensitive to acidic and metamorphic conditions (*e.g.*,
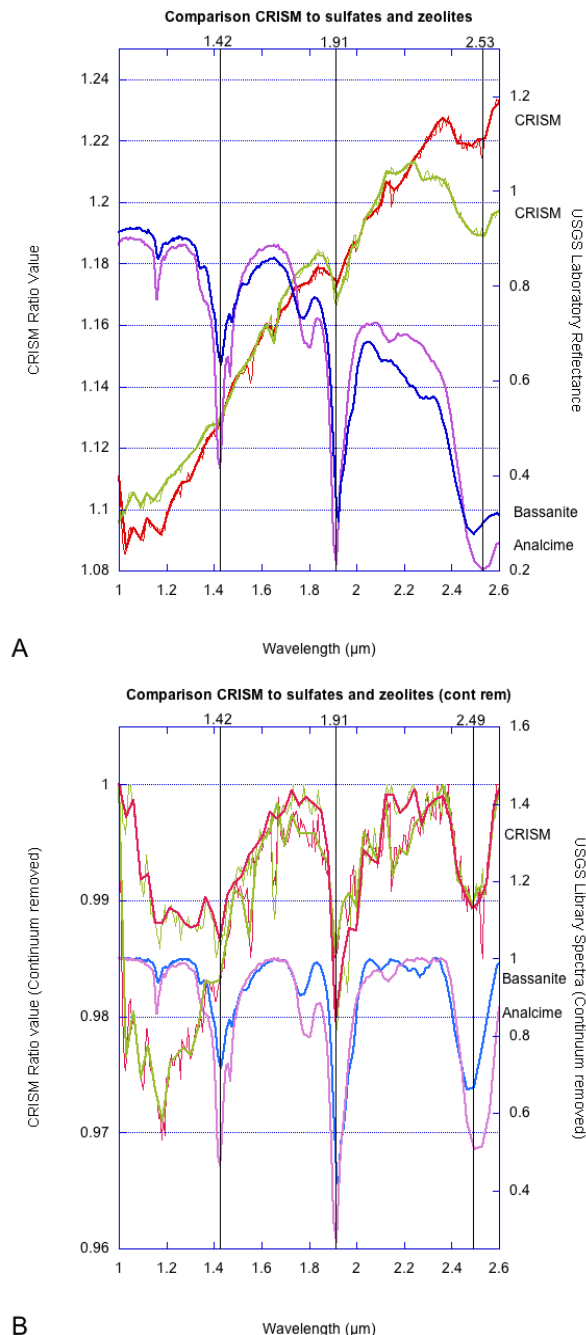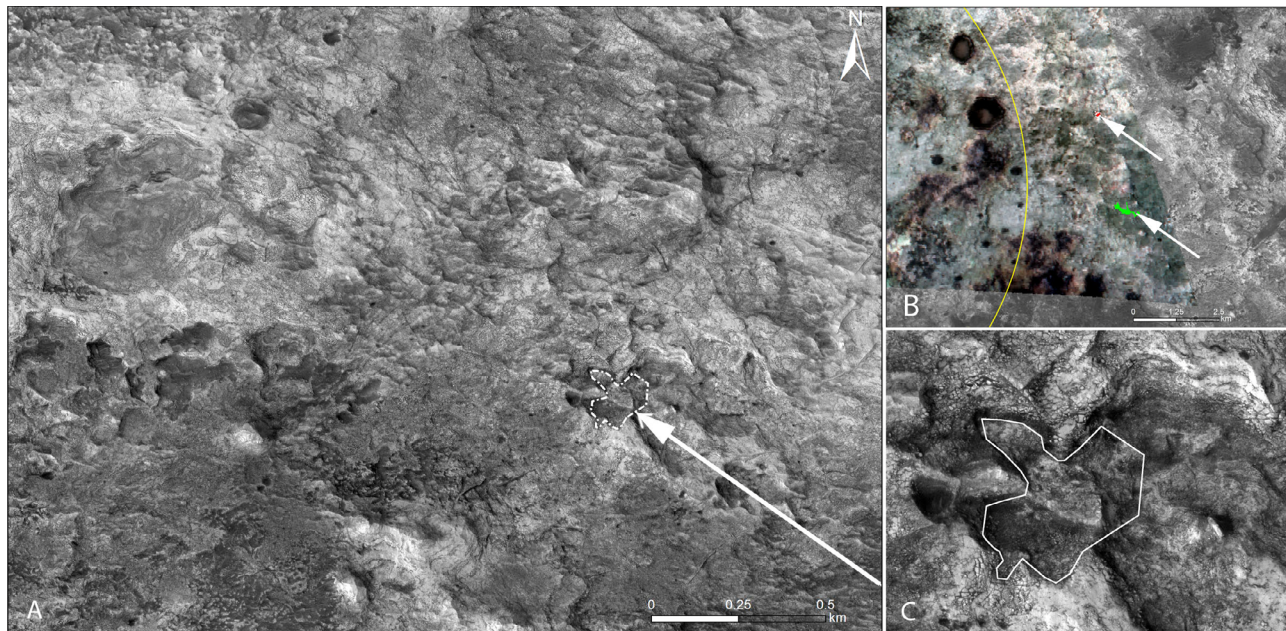
Figure 13. (A) The bassanite/analcime-bearing material is associated with parts of a pitted-and-etched terrain otherwise dominated by the spectrum of Fe-smectites. HiRISE image ESP_012227_2045. (B) Portion of CRISM image FRT0000A600 showing location of units (white arrows). Yellow line denotes boundary of proposed landing ellipse. (C) HiRISE image ESP_012227_2045 showing close-up of bassanite/analcime-bearing unit. The unit appears to underlie the layered Fe-smectites found in the region. (figure13.jpg)

Wilson and Pollard 2002). Hence the best preservation of organics, if they occurred on early Mars, would be found in association with these "pure" occurences of Fe/Mg smectites.

The middle portion of the landing ellipse contains the transition between Fe/Mg smectites and Al-bearing phyllosilicates. This transition is sharp, and has been observed in outcrops at distances of up to 1000 km from the landing ellipse (Noe Dobrea et al. 2010). Hence, its existence is of importance because the spatial scales associated with this transition zone are indicative of regional, if not global processes. A crater that has excavated both units exposes the transition zone, and observations of the walls in this crater can permit analysis of sedimentary bedding, composition, and textures on either side of this transition.

Finally, the western portion of the ellipse will allow us to study the upper Al-phyllosilicate bearing strata that have been proposed to be of diagenetic/pedogenic unit (*e.g.* McKeown et al. 2009; Noe Dobrea et al. 2010). This portion of the landing ellipse is of particular interest because this upper unit has been cut by channels throughout the Mawrth Vallis and western Arabia Terra regions, suggesting that aqueous activity occurred after deposition and perhaps during acid-leaching of this unit (Noe Dobrea et al. 2010).

Conclusions:

We have analyzed CRISM hyperspectral images from the region within and around the proposed Mawrth Vallis MSL landing ellipse. Spectroscopic studies of the rocks exposed in the walls of a pair of nearby craters have allowed us to

identify a stratigraphic section consisting of at least four primary compositional units including two Fe/Mg-smectite rich units at the bottom of the section (units 1 and 2), an Al-phyllosilicate-bearing unit above that (unit 3), and in some areas, an Mg-phyllosilicate-bearing unit above that (unit 4). Spectra of the upper Fe/Mg-smectite-bearing unit (unit 2) typically show clear metal-OH combination bands at 2.29 and 2.38 µm. However, these bands are weak to absent in the lowermost Fe/Mg-smectite-bearing unit although the 1.9 µm hydration band retains the same band-strength, suggesting that the material is mixed with some other hydrated phase. The Al-phyllosilicate bearing unit often has spectral evidence for montmorillonite, beidellite, and kaolinite, as well as other products of acid leaching. Its base shows an enhancement in ferrous phases that may have precipitated from downward migrating Fe^{2+}-rich fluids formed in overlying rocks during acid leaching.

We have noted layering associated with the units exposed in the crater walls (units 1-3) in places where brecciation has not masked their original stratigraphy. Layering is not always flat and may exhibit truncations concave-up bed forms, suggesting a complex depositional environment, possibly sedimentary in at least some of the layers. Additionally, a gradation is observed in the Al-phyllosilicate bearing unit, where fracture patterns are observed near the top of the unit, and layering is observed near the base, usually in association with the ferrous portion of the unit. It is difficult to attribute this morphologic change soley to impact forces during crater formation.

Additional spectroscopic analyses of CRISM observations east of the proposed landing ellipse have also revealed the presence of a hydrated material that has a broad, rounded
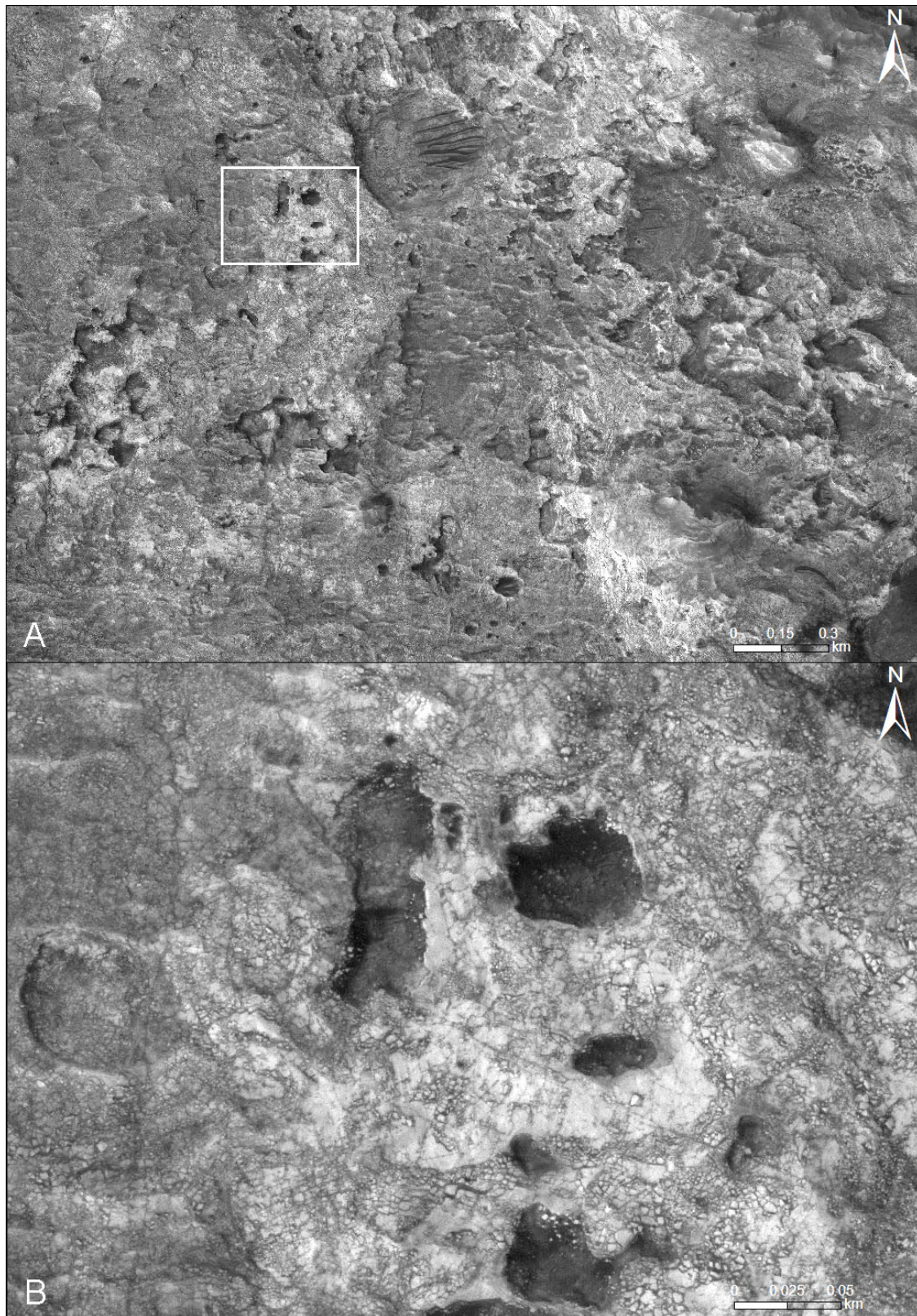
41

Figure 14. (A) Another example of pitted-and-etched terrain in the area east of the proposed landing ellipse. White box shows location of B. HiRISE image ESP_012227_2045. (B) Close-up of white box. Pits exist in a variety of shapes, present no rims, and have boulders lying in their interior, suggesting that they formed form collapse.
(figure14.jpg)

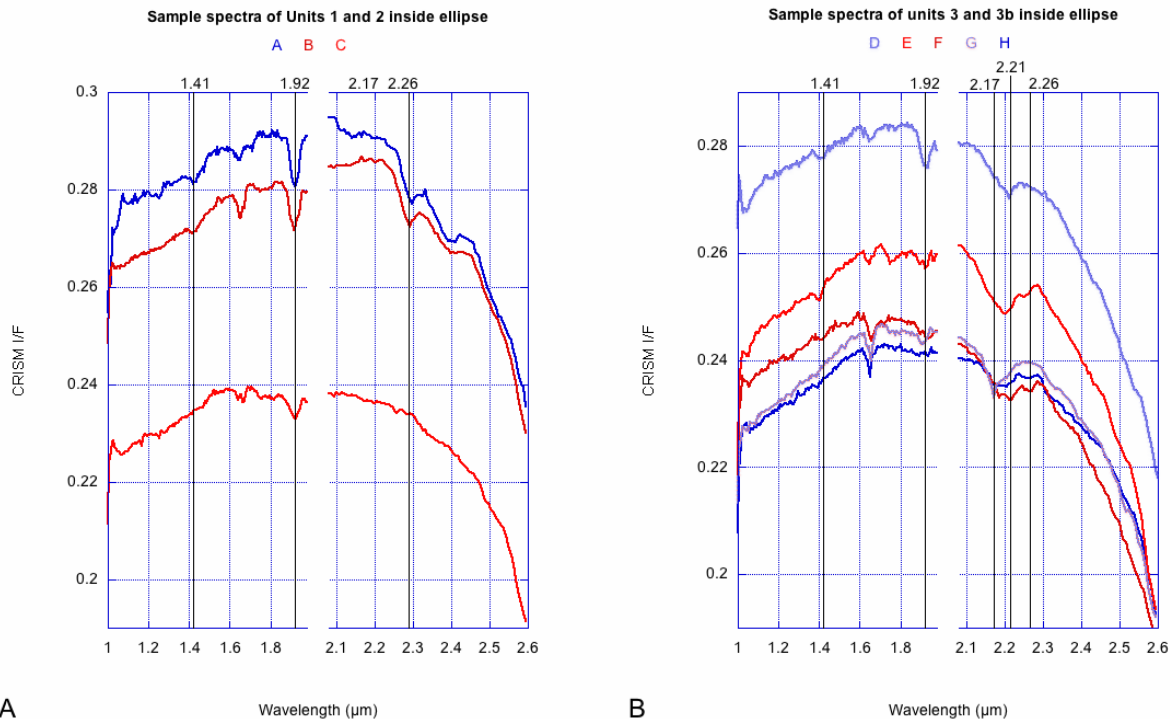**Figure 15.** (A) Spectra of units 1 and 2 from areas inside the landing ellipse. (B) Spectra of unit 3 and subunit 3b from areas inside the landing ellipse. Colored letters indicate location of spectra in Figure 16. (figure15.gif)

spectral absorption near 2.5 µm. Although both bassanite and analcime are consistent with the observed spectra, we have interpreted this spectral signature to be due to bassanite based on this area's proximity to previously identified bassanite locations and the notable morphological setting it is found in at this location. Stratigraphically, the unit bearing this material appears to underlie the layered Fe/Mg smectite-bearing units. This putative bassanite-bearing horizon is characterized by a pitted-and-etched morphology, which we interpret to be the result of dissolution of sulfates by groundwater activity or dehydration of gypsum during burial.

Evidence of a variety of environmental conditions appear to be preserved in the rocks within the landing ellipse, with Fe/Mg-smectites preserving evidence for more neutral conditions exposed primarily in the eastern portion of the ellipse, and Al-phyllosilicates preserving evidence for more acidic conditions occurring dominantly in the western portion of the ellipse. The boundary between these two mineralogical units is sharp, well exposed, and easily accessible to a rover. The putative sulfate-bearing horizon is easily accessible a few hundred meters east of the ellipse. Overall, the proposed MSL landing ellipse and immediate surroundings contain a bounty of material that may span a broad range of the Noachian and Early Hesperian epochs, including periods of neutral to acidic aqueous conditions on the martian surface. The units dating to this time period are present over much of the exposed surface, are easily accessible, and contain unambiguous evidence for aqueous

alteration under a range of conditions relevant to understanding climate change and habitability of the Martian surface.

Directory of supporting data

root directory
    noe_dobrea_mars_2011_0003.pdf this file
    Full-resolution images
        Fig. 1 figure1.jpg
        Fig. 2a figure2a.gif
        Fig. 2b figure2b.gif
        Fig. 4a figure4a.gif
        Fig. 4b figure4b.gif
        Fig. 5 figure5.gif
        Fig. 6 figure6.jpg
        Fig. 7 figure7.jpg
        Fig. 8 figure8.gif
        Fig. 9 figure9.gif
        Fig. 10a figure10a.gif
        Fig. 10b figure10b.gif
        Fig. 11 figure11.gif
        Fig. 12a figure12a.gif
        Fig. 12b figure12b.gif
        Fig. 13 figure13.jpg
        Fig. 14 figure14.jpg
        Fig. 15 figure15.gif
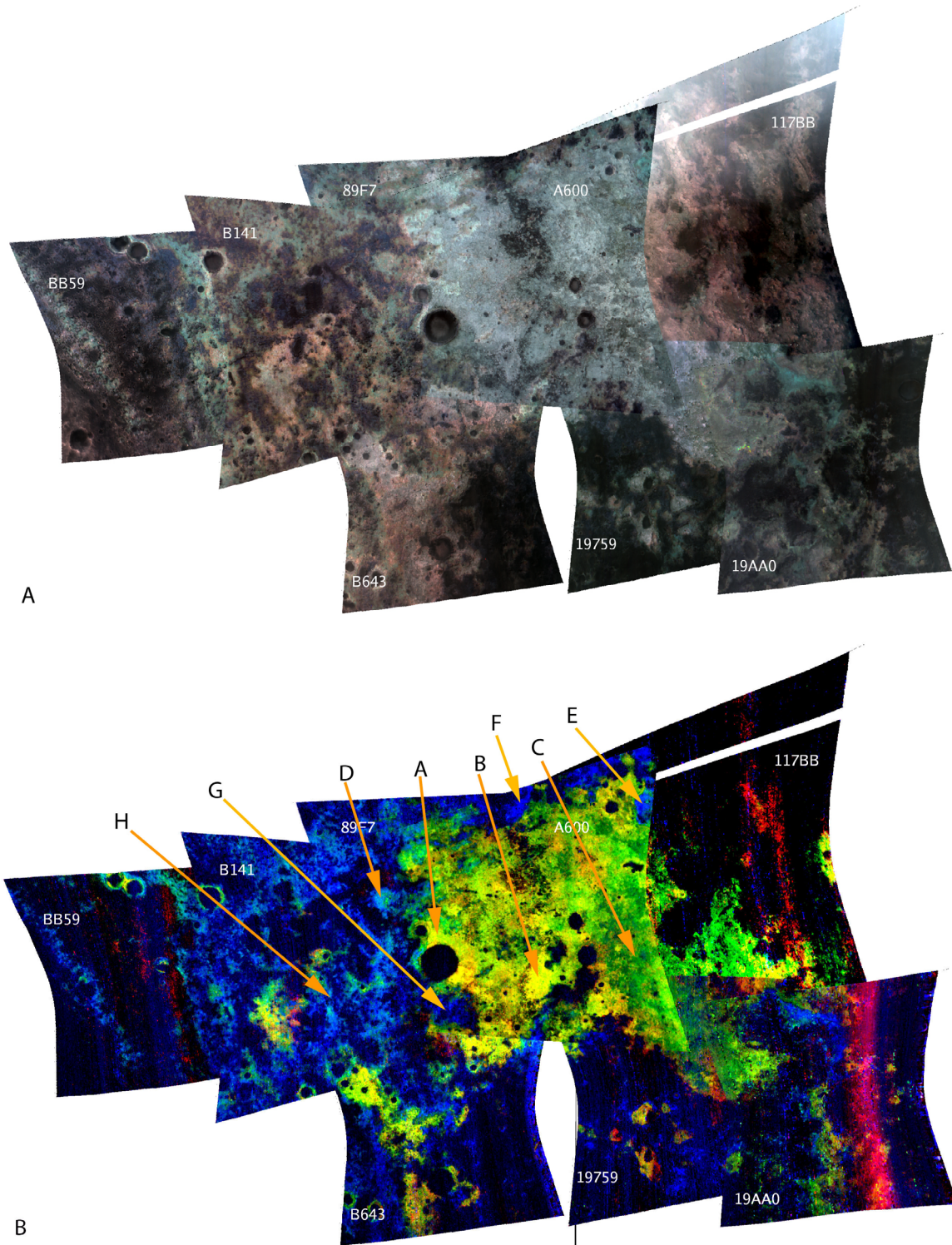   Fig. 16a figure16a.jpg
        Fig. 16b figure16b.jpg

Figure 16. (A) RGB IR-composite mosaic of the CRISM FRT observations falling within the proposed landing ellipse. R= 2.53 µm, G=1.51 µm, B=1.08 µm. (B) RGB composite mosaic of the parameter maps for the types identified in image FRT000094F6, where R=D2300, G=BD1900R, B=BD2200. Stretch thresholding of the images was done by setting the lower threshold of each parameter map to 0, and by defining the higher threshold by eye to accentuate the color differences and smooth transition between images. These color units were then checked against actual spectra to confirm that the colors map the units as defined in this paper. Labeled arrows reference spectra in Figure 15. (figure16a.jpg) (figure16b.jpg)

Acknowledgements

References

Altheide, T. S., V. Chevrier and E. Noe Dobrea (2010) "Mineralogical characterization of acid weathered phyllosilicates with impications for secondary martian deposits" Geochimica Et Cosmochimica Acta 74, 6232-6248. doi:10.1016/j.gca.2010.08.005

Bibring, J.-P. Y. Langevin, J. F. Mustard, F. Poulet, R. Arvidson, A. Gendrin, B. Gondet, N. Mangold, P. Pinet and F. Forget (2006) "Global mineralogical and aqueous Mars history derived from OMEGA/Mars Express data" Science 312, 400-404. doi:10.1126/science.1122659

Bishop, J. L., P. Schiffman, M. D. Lane and M. D. Dyar (2005) "Solfataric alteration in Hawaii as a mechanism for formation of the sulfates observed on Mars by OMEGA and the MER instruments" Lunar and Planetary Science XXXVI, Abstract No. 1456, League City.

Bishop, J. L. et al. (2008) "Phyllosilicate diversity and past aqueous activity revealed at Mawrth Vallis, Mars" Science 321, 1159830. doi:10.1126/science.1159699

Bishop, J. L., M. D. Lane, M. D. Dyar and A. J. Brown (2008b) "Reflectance and emission spectroscopy study of four groups of phyllosilicates: Smectites, kaolinite, serpentines, chlorites and micas" Clay Minerals 43, 35. doi:10.1180/claymin.2008.043.1.03

Bishop, J. L. et al. (2009) "Mineralogy of Juventae Chasma: Sulfates in the light-toned mounds, mafic minerals in the bedrock, and hydrated silica and hydroxylated ferric sulfate on the plateau" Journal of Geophysical Research 114, E00D09. doi:10.1029/2009JE003352

Chipera, S. J. and D. T. Vaniman (2007) Experimental stability of magnesium sulfate hydrates that may be present of Mars, Geochimica et Cosmochimica Acta 71, 241. doi: 10.1016/j.gca.2006.07.044

Churchman, G. J. and R. M. Carr (1975) "The definition and nomenclature of halloysites" Clays and Clay Minerals 23, 382-388.

Clark, R. N., G. A. Swayze, R. Wise, K. E. Livo, T. M. Hoefen, R. F. Kokaly and S. J. Sutley (2007) United States Geological Survey Digital Spectral Library splib06a, United States Geological Survey Digital Data Series DS-231.

Ehlmann, B. L. et al. (2009) "Identification of hydrated silicate minerals on Mars using MRO-CRISM: Geologic context near Nili Fossae and implications for aqueous alteration" Journal of Geophysical Research 114, E00D08. doi:10.1029/2009JE003339

Farrand, W. H., T. D. Glotch, J. W. Rice Jr., J. A. Hurowitz and G.A. Swayze (2009) "Discovery of jarosite within the Mawrth Vallis region of Mars: Implications for the geologic history of the region" Icarus 204, 478–488. doi:10.1016/j.icarus.2009.07.014

Kraft, M. D., J. R. Michalski, C. Jones, S. S. Murray and D. M. Worrall (2003) "Thermal emission spectroscopy of the silica polymorphs and consideration for remote sensing of Mars" Geophysical Research Letters, 30, 2008. doi:10.1029/2003GL018354

Langevin, Y., F. Poulet, J.-P. Bibring, B. Schmitt, S. Douté and B. Gondet (2005) "Summer evolution of the north polar cap of Mars as observed by OMEGA/Mars Express" Science 307, 1581-1584.

doi:10.1126/science.1109438

Mangold, N. et al. (2008) "Spectral and geological study of the sulfate-rich region of West Candor Chasma, Mars" Icarus 194, 519-543. doi:10.1016/j.icarus.2007.10.021

McKeown, N. K., J. L. Bishop, E. Z. Noe Dobrea, M. Parente, B. L. Ehlmann, J. F. Mustard, S. L. Murchie, G. Swayze, J.-P. Bibring and E. Silver (2009) "Characterization of phyllosilicates observed in the central Mawrth Vallis region, Mars, their potential formational processes, and implications for past climate" Journal of Geophysical Research 114, E00D10. doi:10.1029/2008JE003301

Michalski, J. R. and E. Z. Noe Dobrea (2007) "Evidence for a sedimentary origin of clay minerals in the Mawrth Vallis region, Mars" Geology 35, 951-954. doi:10.1130/G23854A.1

Michalski, J. R. and R. L. Fergason (2009) "Composition and thermal inertia of the Mawrth Vallis region of Mars from TES and THEMIS data" Icarus 199, 25-48. doi:10.1016/j.icarus.2008.08.016

Michalski, J. R. et al. (2010) "The Mawrth Vallis region of Mars: A potential landing site for the Mars Science Laboratory (MSL) mission" Astrobiology 10, 687-703. doi:10.1089/ast.2010.0491

Mirwald, P. W. (2008) "Experimental study of the dehydration reactions gypsum-bassanite and bassanite-anhydrite at high pressure: Indication of anomalous behavior of H_2O at high pressure in the temperature range of 50-300°C" Journal of Chemical Physics 128. doi:10.1063/1.2826321

Mustard, J. F. et al. (2008) "Hydrated silicate minerals on Mars observed by the Mars Reconnaissance Orbiter CRISM instrument" Nature 454, 305-309. doi:10.1038/nature07097

Noe Dobrea, E. Z. et al. (2008) "Correlations between hematite and sulfates in the chaotic terrain east of Valles Marineris" Icarus 193, 516-534. doi:10.1016/j.icarus.2007.06.029

Noe Dobrea, E. Z. et al. (2010) "Mineralogy and stratigraphy of phyllosilicate-bearing and dark mantling units in the greater Mawrth Vallis/west Arabia Terra area: Constraints on geological origin" Journal of Geophysical Research 115, E00D19. doi:10.1029/2009JE003351

Parente, M. (2008) "A new approach to denoising CRISM images" Lunar Planetary Science Conference XXXIX, Abstract No. 1391, League City.

Pelkey, S. M. et al. (2007) "CRISM multispectral summary products: Parameterizing mineral diversity on Mars from reflectance" Journal of Geophysical Research 112, E08S14. doi:10.1029/2006JE002831

Poulet, F., J.-P. Bibring, J. F. Mustard, A. Gendrin, N. Mangold, Y. Langevin, R. E. Arvidson, B. Gondet and C. Gomez (2005) "Phyllosilicates on Mars and implications for early martian climate" Nature 438, 623-627. doi:10.1038/nature04274

Poulet, F. et al. (2008) "Mineralogy of Terra Meridiani and western Arabia Terra from OMEGA/MEx and implications for their formation" Icarus 195, 106. doi:10.1016/j.icarus.2007.11.031

Roach L. H., J. F. Mustard, G. Swayze, R. E. Milliken, J. L. Bishop, S. L. Murchie and K. Lichtenberg (2010) "Hydrated mineral stratigraphy of Ius Chasma, Valles Marineris" Icarus 206, 253-268. doi:10.1016/j.icarus.2009.09.003

Tosca, N. J., R. E. Milliken and F. M. Michel (2008) "Smectite formation on early Mars: experimental constraints" Workshop on Martian Phyllosilicates: Recorders of Aqueous Processes, LPI Contribution No. 1441, 77-78, Paris.

Weitz, C. M., E. Z. Noe Dobrea, R. M. E. Williams, J. Metz, C. Quantin, M. Parente and J. Grotzinger (2009) "MRO observations of fluvial features, sulfates, and other landforms in the Melas Chasma basin" Lunar Planetary Science Conference XL, Abstract No. 1874, The Woodlands.

Wilson, L. and M. Pollard (2002) "Here today, gone tomorrow? Integrated experimentation and geochemical modeling in studies of archaeological diagenetic change" Accounts of Chemical Research, 35, 644-651. doi:10.1021/ar000203s

Wray, J. J., S. W. Squyres, L. H. Roach, J. L. Bishop, J. F. Mustard and E. Z. Noe Dobrea (2010) "Identification of the Ca-sulfate bassanite in Mawrth Vallis, Mars" Icarus 209, 416-421. doi:10.1016/j.icarus.2010.06.001